ARTICLE OPEN

Check for updates

Individualized therapy guided by single-cell sequencing in anti-$GABA_AR$ encephalitis

Yaqing Shu[1✉], Yu Huang[1], Qihui Li[1], Huilu Li[1], Zhibin Li[1], Jinlong Ye[2], Jianning Chen[3], Jianfang Li[4], Ling Fang[5], Jing Li[1], Yi Lu[6], Libao Liu[7], Yongjian Luo[8], Zhanhang Wang[2], Zhengqi Lu[1], Zhongxi Huang[9✉], Fuhua Peng[10✉] and Wei Qiu[1✉]

We presented a patient with refractory anti-$GABA_A$-R encephalitis, and constructed libraries for single-cell sequencing from the patient's peripheral blood mononuclear cells (PBMCs), cerebrospinal fluid cells, as well as four healthy volunteer's PBMCs. A distinct group of monoclonal $CD8^+$ T cells and an abnormal JAK-STAT signaling pathway was implicated in the disease. The cross-reactive protein LIM-domain-only protein 5 (LMO5) identified in the patient's thymoma, prompted the activation of the specific $CD8^+$ T cells. Furthermore, in vitro analysis revealed the involvement of the JAK-STAT pathway in LMO5-induced $CD8^+$T cell activation, a process effectively suppressed by tofacitinib, which improved the patient's clinical outcome.

Translational Psychiatry (2025)15:78 ; https://doi.org/10.1038/s41398-025-03300-y

INTRODUCTION

Encephalitis linked to antibodies against the neuronal g-aminobutyric acid type A ($GABA_A$) receptor ($GABA_A$-R) constitutes a rare, distinctive, and severe form of autoimmune encephalitis [1, 2]. The etiology and pathomechanisms of anti-$GABA_A$-R encephalitis remain elusive. While immune therapy shows favorable responses in some cases, a subset of patients experiences poor outcomes [2], indicating a pressing need for personalized medicine in the management of anti-$GABA_A$-R encephalitis.

METHODS AND MATERIALS

Statement of ethics

The protocol of study was approved by the Ethics Committee of the Third Affiliated Hospital of Sun Yat-Sen University ([2021]02-014-01) and carried out in accordance with the principles described in Declaration of Helsinki of 1975.

Index patient and clinical history

The patient, a 42-year-old male, initially presented with psychiatric disorders followed by loss of consciousness, fever, and seizures, persisting for a month despite treatment with steroid and multiple antiepileptic drugs (AEDs). Upon admission to our hospital, he was in a comatose state with a tracheotomy, exhibiting a Glasgow Coma Scale (GCS) score of 8 (E4V2M2), a modified Rankin Scale (mRS) of 5, and Clinical Assessment Scale in Autoimmune Encephalitis (CASE) score of 20 (Fig. 1A, Supplemental table 1, the scores of the patient were assessed while maintaining blinding procedures). *Pseudomonas aeruginosa* pneumonia was identified through sputum culture and next-generation sequencing (NGS). Cerebrospinal fluid (CSF) analysis indicated elevated white blood cells (WBC) at 5/μL and total protein at 371 mg/dL. In the CSF, viral, fungal, and bacterial polymerase chain reactions and cultures were negative, and no malignant cells were found. CSF was also collected for PACEseq metagenomic next-generation sequencing (mNGS) detection, while the result was negative.

Positive serum and CSF anti-$GABA_A$ antibody (titer, serum 1:30, CSF 1:30) were detected using a cell-based assay with HEK293 cells transfected with plasmids encoding $GABA_A$. Other autoimmune encephalitis antibodies and serological tests for anti-myelin oligodendrocyte (MOG), glial fibrillary acidic protein (GFAP), and aquaporin 4 (AQP4) were negative (Supplemental Fig. 2A, B). Coagulation analysis revealed abnormal activated partial thromboplastin time (APTT, 142.3 seconds) and deceased Factor XII viability (0.1%, normal range 70–150%). Whole genome sequencing of DNA in the patient's white blood cells detected an *F12* mutation (Supplemental Fig. 4; Supplemental table 6).

Brain magnetic resonance imaging (MRI) revealed increased T2/FLAIR signal with extensive cortical-subcortical-basal ganglia involvement and leptomeningeal enhancement (Fig. 1A(a, b)). Electroencephalogram (EEG) indicated the presence of rhythmic periodic sharp-slow waves in the bilateral temporo-frontal areas (Supplemental Fig. 1A). Positron Emission Tomography with Computed Tomography (PET/CT) scans indicated increased fluorodeoxy-D-glucose (FDG) uptake in the left-sided mediastinal mass, revealing a mediastinal tumor (Fig. 1C).

Due to the patient's severe condition and coagulation abnormalities, surgical intervention for the mediastinal tumor was deemed intolerable. Treatment involved prednisolone, intravenous immunoglobulin (IVIG), and anti-epileptic drugs (AEDs). However, the patient exhibited limited response to immune therapy and subsequently developed gastrointestinal bleeding (Fig. 1A). As gastrointestinal bleeding and severe pneumonia, the steroid treatment also was interrupted.

Considering the patient's low peripheral blood B cell levels, with a CD3-CD19 + B cell to lymphocyte ratio of 3.53%, which falls below the normal

[1]Department of Neurology, The Third Affiliated Hospital of Sun Yat-sen University, Guangzhou, China. [2]Department of Neurology, GuangDong 999 Brain Hospital, Guangzhou, China. [3]Department of Pathology, The Third Affiliated Hospital of Sun Yat-sen University, Guangzhou, China. [4]Department of Nuclear Medicine, The Third Affiliated Hospital of Sun Yat-sen University, Guangzhou, China. [5]Department of Radiology, The Third Affiliated Hospital of Sun Yat-sen University, Guangzhou, China. [6]Department of Neurology, The Eighth Affiliated Hospital, Sun Yat-sen University, Shenzhen, China. [7]Department of Cardiothoracic surgery, The Third Affiliated Hospital of Sun Yat-sen University, Guangzhou, China. [8]SequMed Institute of Biomedical Sciences, Guangzhou, China. [9]Cancer Research Institute, School of Basic Medical Sciences, Southern Medical University, Guangzhou, China. [10]The Academician Workstation, Jiangxi University of Chinese Medicine, Nanchang, China. ✉email: shuyaq@mail.sysu.edu.cn; zxhuang@smu.edu.cn; pengfuhua@jxutcm.edu.cn; qiuwei@mail.sysu.edu.cn

Received: 11 August 2024 Revised: 16 January 2025 Accepted: 24 February 2025
Published online: 08 March 2025

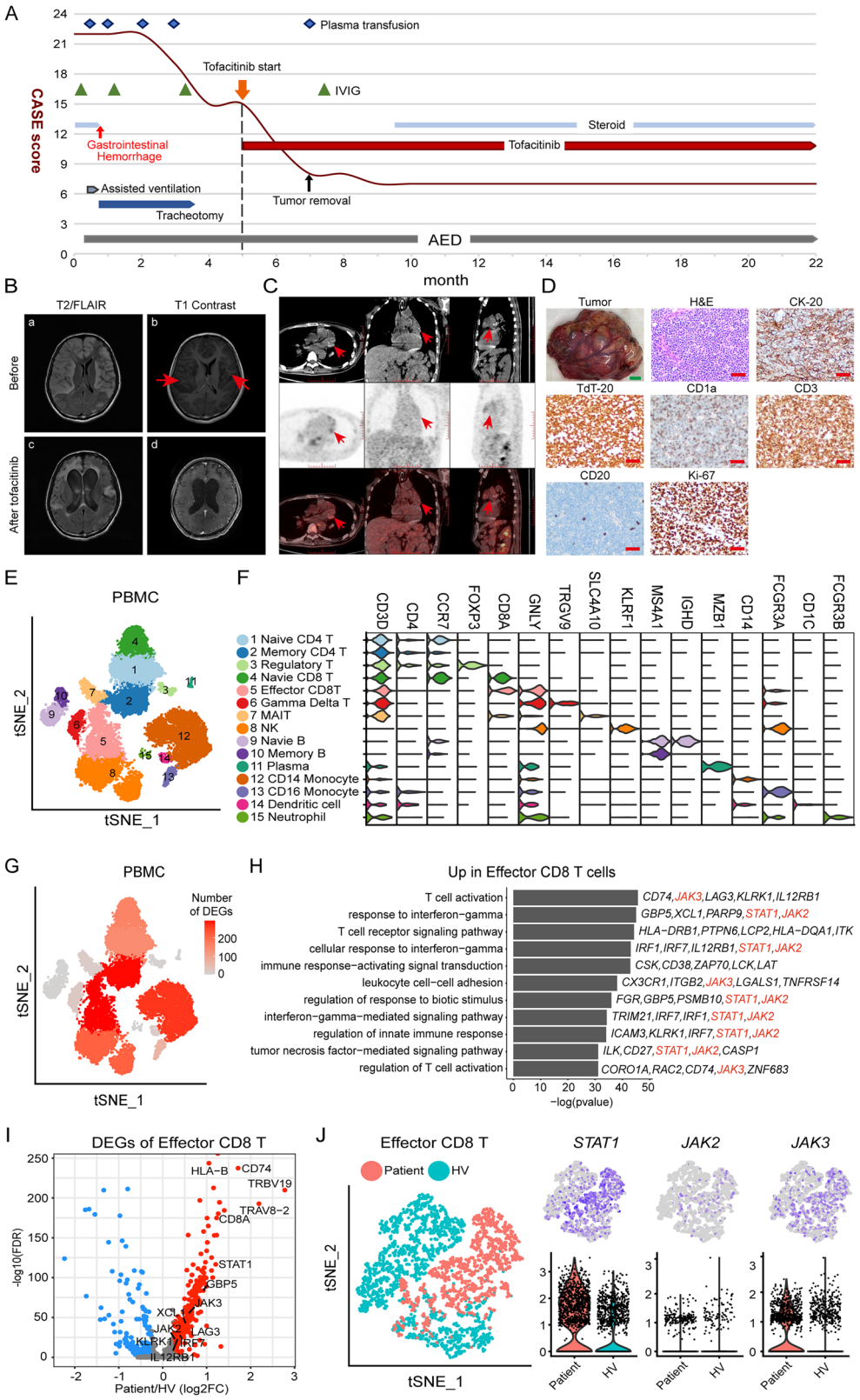

range of 5–18%, coupled with the presence of severe pneumonia, it was determined that rituximab would not be administered.

Given the potential of scRNA-seq to enhance the understanding of pathological processes in human diseases, scRNA-seq was performed during the subsequent treatment process.

Single-cell isolation and library development

Libraries for scRNA-seq from the patient peripheral blood mononuclear cells (PBMCs) and CSF cells, as well as one healthy volunteer (HV)-PBMC, were constructed using a Single Cell 5′ Library and Gel Bead kit (10× Genomics, cat# 1000014) and Chromium Single Cell V(D)J Enrichment Kits,

Fig. 1 Clinical course, treatment history, and scRNA-seq analysis in PBMCs derived from the index patient. A Clinical presentation and progression prior to and after intervention using the JAK inhibitor tofacitinib. IVIG, intravenous immunoglobulin; AED, antiepileptic drug including Pirenpanet, Valproate, Midazolam, Clonazepam, topiramate, Levetiracetam. **B** Brain magnetic resonance imaging (MRI) of the patient prior to or following tofacitinib treatment. Elevated T2/FLAIR signal intensities in extensive cortical-subcortical-basal ganglia (a) with leptomeningeal enhancement in the gadolinium-enhanced T1-weighted image (b, red arrows) before treatment. After tofacitinib treatment, the images have clearly improved (c, d). **C** PET-CT images from the patient. PET-CT images illustrating abnormal metabolism in the mass on the left side of the upper mediastinum, as indicated by the arrow. **D** H&E staining of thymoma and immunohistochemistry of CK-20, TdT-20, CD1a, CD3, CD20, and Ki67 within thymoma. **E** The t-SNE plot projection including 6338 cells from anti-$GABA_A$ receptor encephalitis patient peripheral blood mononuclear cells (PBMCs) and 16,551 cells obtained from healthy volunteer (HV) PBMCs, shaded based on their cell type. **F** Violin plots depicting the normalized expression levels of cluster-defining genes across individual clusters. The columns represent selected marker genes, and the rows represent clusters with the same color as identified in E. **G** t-SNE plot illustrating the number of differentially expressed genes (DEGs) across patient and HV cells within each cluster. DEGs were identified using a Wilcoxon test, with a threshold of $|\log_2$ fold change$|$ >0.25; adjusted p-value $<10^{-12}$. **H** GO enrichment analyses of the DEGs. Bar plot showing the upregulated GO term in Effector CD8 T cells, and notable genes are labeled in red. The p-value was derived using a hypergeometric test. **I** Volcano plot depicting DEGs that are up- or down-regulated in Effector CD8 T cells, with relevant DEGs labeled. **J** Effector CD8 T cells ($n = 2890$ cells) were projected onto a t-SNE plot colored by origin (left). Expression of selected genes was projected onto the t-SNE plot (top), and the violin plots show the expression levels (bottom).

Human (10× Genomics, cat# 1000005, 1000016) using the manufacturer's instructions.

The remaining three healthy volunteer (HV)-PBMC cell suspensions were resuspended in a Labeling Buffer with PBS containing 1% BSA. Human TruStain FcX™ Antibody (Biolegend, cat# 422301) was added and incubated, and various hashtag antibodies were added to each sample. Following incubation, the samples were washed, resuspended, and mixed using a Single Cell 3′ Library and Gel Bead kit (10× Genomics, cat# 1000092) and Chromium Single Cell B Chip kit (10× Genomics, cat# 1000074). The cell suspension was loaded onto a Chromium single-cell controller (10× Genomics) to construct single-cell gel beads within the emulsion (GEMs). Isolated cells were lysed, and the released RNA was barcoded via reverse transcription within individual GEMs. Reverse transcription was conducted using a C1000TM Touch Thermal Cycler (Bio Rad) at 53 °C for 45 min, followed by 85 °C for 5 min, and a hold at 4 °C. Complementary DNA was produced and amplified, and cDNA was separated for 3′ gene expression library and cell surface protein library development using SPRIselect.

The libraries were sequenced utilizing an Illumina Novaseq6000 sequencer and a paired-end 150-bp (PE150) approach.

ScRNA-seq analysis

Single-cell RNAseq data were treated using CellRanger (v.5.0.0) with the GRCh38 human reference. Downstream analyses were performed using filtered gene expression matrices in R (v.4.0.4) utilizing the Seurat package (v.4.0.5). Briefly, after removing doublet or negative cells with the HTODemux function, for quality control, cells with (1) gene count <500; (2) UMI count <800; (3) mitochondrial gene proportion >20%, were removed as low-quality cells. For identification and comparison of shared cell types, we used the SCTransform and IntegrateData standard workflows for normalization, variable gene selection, integration, dimensionality reduction, and clustering, as outlined online (https://satijalab.org/seurat/articles/integration_introduction). For clustering, we employed FindNeighbours and FindClusters functions on 30 PCA components using a resolution of 0.7, and t-Distributed Stochastic Neighbor Embedding (t-SNE) dimensionality reduction was conducted using the first 30 PCA components to acquire a 2-dimensional representation of the cellular states. To characterize the clusters, the FindAllMarkers function was employed to identify cluster-specific gene expression, based on the clusters classified and annotated. Differential gene expression was examined using the FindMarkers function in Seurat alongside the Wilcoxon Rank Sum test with default parameters, and the Benjamini-Hochberg method was utilized to assess the false discovery rate (FDR). DEGs were filtered with a minimum log2(fold change) of 0.25 and a maximum FDR value of 0.05, and enrichment analysis for the functions of the DEGs was performed using the clusterProfiler package.

TCR V(D)J sequencing and analysis

Single-cell TCR V(D)J data were handled using CellRanger (v.5.0.0) with GRCh38 VDJ for demultiplexing, gene quantification, and TCR clonotype assignment. A TCR diversity metric containing clonotype frequency and barcode information was generated. Using the barcode information, T cells with prevalent TCR clonotypes were projected onto a t-SNE plot.

Whole genome sequencing (WGS)

WGS was performed on white blood cells from the patient, and was performed with 50× coverage using BGI MGISEQ-T7 and standard protocols. Sequence reads were mapped to the human reference genome Hg38. SNPs and InDels were identified using GATK (Genome Analysis TK 4.2.3.0).

LMO5-TCR docking analysis

ColabFold, ZDOCK, PyMol, and other tools were utilized to simulate docking between LIM-domain-only protein 5 (LMO5) and the top 10 TCR clonotypes to assess if an interaction between LMO5 and TCR was possible. Specifically, ColabFold was used to calculate the protein structures of TCR by combining Mmseqs2 with AlphaFold2. Protein docking was predicted with ZDOCK, and the outcome was visualized using PyMol.

Dot blot

A nitrocellulose membrane premoistened with tris-buffered saline (TBS) was utilized in a Bio-Dot apparatus (706,545, Bio-Rad, Richmond, CA, USA), and 100 µL of recombinant LMO5 protein (0.18 µg/mL; Alpalife, Shenzhen, Guangdong, China) was added. After the peptide solution was completely filtered through the membrane, the wells were blocked using 100 µL of 2% bovine serum albumin (BSA; 155,681, Jackson ImmunoResearch, West Grove, PA, USA) in TBS-0.05% Tween-20 (TBST) at room temperature until draining of the blocking solution. Thereafter, 100 µL of serum (1:1000 in TBST), or100 µL of anti-LMO5 antibody (serving as a positive control, 1:1000 dilution in TBST, ab178695, abcam) was added onto the membrane for 1 h at room temperature. The wells were washed three times using 400 µL of TBST. Subsequently, the wells were incubated with 200 µL of HRP-conjugated anti-human IgG secondary antibody (1:10000; bs-0297G-HRP, Bioss, Shanghai, China), anti-rabbit IgG secondary antibody (1:2000; 111-035-003, Jackson ImmunoResearch) for 1 h at room temperature. The membrane was removed from the apparatus and rinsed with TBST three times (10 min each). Dots were assessed using Immobilon Western chemiluminescent HRP substrate (WBKLS0500, Merck, Darmstadt, German), and images were obtained with an ImageQuant LAS 4000 (GE Healthcare Life Sciences, Issaquah, WA, USA).

Hematoxylin and eosin (H&E) staining

Paraffin-embedded tissues were sectioned into 3 µm thick slices. H&E staining was conducted based on the standard protocol. Briefly, sections underwent the following steps: dewaxing (xylene, 2 × 2 min), rehydration (90% ethanol for 10 min, 80% ethanol for 10 min, and 75% ethanol for 10 min), hematoxylin staining (5 min, G1004, Servicebio, Wuhan, Hubei, China), differentiation (2 s, G1039, Servicebio), bluing (2 seconds, G1040, Servicebio), dehydration (85% ethanol for 5 min and 95% ethanol for 5 min), eosin staining (5 min, G1001, Servicebio), dehydration (anhydrous ethanol for 3 × 5 min), and clearing (xylene, 2 × 5 min). Sections were then sealed using neutral gum (10,004,160, Sinopharm, Beijing, China) and photographed using an Olympus IX-71 inverted fluorescent microscope (Olympus, Tokyo, Japan).

Immunohistochemistry

Paraffin-embedded sections (3 µm thick) were dewaxed using xylene and heated within 0.01 M sodium citrate buffer (pH = 6.0) in a microwave at

60 °C for 20 min for antigen retrieval. Tissue sections were blocked in 0.3% H_2O_2 for 10 min to stop endogenous peroxidase activity, followed by incubation with a primary antibody against LMO5 (1:100; 10892-2-AP, proteintech), CK-20 (1:100; AQ20029, aq-meditech), TdT-20 (ready-to-use; RMA-1044, MXB Biotechnologies), CD1a (1:50; MAB-0336, MXB Biotechnologies), CD3 (1:100; AQ20001, aq-meditech), CD20 (ready-to-use; Kit-0001, MXB Biotechnologies), or Ki67 (1:100; MAB-0672, MXB Biotechnologies). The target was assessed using a DAB staining kit (GK600710, Gene Tech, Shanghai, China).

Western Blot

The diluted serum (1:6) or CSF was combined with 4× SDS sample loading buffer and denatured at 95 °C for 10 min. The samples were separated using sodium dodecyl sulfate-polyacrylamide gel electrophoresis (SDS-PAGE) and transferred onto a polyvinylidene difluoride (PVDF) membrane. The PVDF membrane was blocked using 5% nonfat dry milk in TBST for 2 h at room temperature, then incubated with anti-LMO5 antibody (1:1000) overnight at 4 °C, and incubated with anti-rabbit IgG secondary antibody (1:5000; BA1054, BOSTER) for 1 h at room temperature. The bands were visualized using BeyoECL plus (P0018, Beyotime Biotechnology), and images were acquired utilizing Tanon-4100 (Tanon, China). ImageJ software was employed to quantify the band intensity.

Immunoprecipitation

Immunoprecipitation was performed using a commercialized immunoprecipitation kit (IEMed-K206, IEMed) according to the manufacturer's instructions. Briefly, 50 mL AB binding buffer was added into a microcentrifuge tube containing 10 mL Protein A/G beads. The tube was placed on a magnetic stand for 1 min. The supernate was discarded and the beads were incubated with 100 mL of AB binding buffer and 2 mg of human IgG on a rotating platform for 30 min at room temperature. Then, the beads were collected using the magnetic stand and incubated with denatured serum or CSF on a rotating platform for 1 h at room temperature. Following washing with IP washing buffer, proteins were eluted from the beads with 100 mL of WB elution buffer.

ELISA test

96-well microplates were coated with anti-LMO5 antibody (10 mg/mL; ab178695, abcam) for 16 h at 4 °C. The wells were rinsed with PBS (wash buffer) three times and incubated with 100 mL LMO5 recombinant protein (at concentrations of 600 ng/mL, 300 ng/mL, 150 ng/mL, 75 ng/mL, 37.5 ng/mL, 18.8 ng/mL, 9.4 ng/mL), CSF, or serum at 37 °C for 1 h. After washing with 200 mL of wash buffer three times, the plates were sequentially incubated with an anti-LMO5 antibody (A7549, ABclonal) and horseradish peroxidase (HRP)-conjugated secondary antibody (AS014, ABclonal) at 37 °C for 1 h. A sample of 100 mL TMB substrate (AR1104, Boster) was added to each well, and the plate was incubated in the dark at 37 °C for 15 min. Subsequently, 50 mL of stop solution (AR1105, Boster) was employed to stop the reaction. Optical densities (ODs) were measured at 450 nm using a Victor X5 Series Multilabel Plate Reader (PerkinElmer, USA).

Lymphocyte transformation test (LTT) and flow cytometry examination

Isolated PBMCs were resuspended in PBS and incubated with 5 mM CFSE (C34554, Invitrogen) for 20 min at room temperature. Complete medium containing RPMI-1640 medium, fetal bovine serum (FBS, 10%), penicillin (100 U/mL), and streptomycin (100 mg/mL) was added to the reaction for 5 min at room temperature to remove the free dye. An aliquot of 2.5×10^5 PBMCs was cultivated in a 96-well plate in 200 mL of complete medium with or without 50 ng/mL of LMO5 or 40 nM tofacitinib. Following incubation at 37 °C for 6 days without changing the medium, the PBMCs were stained using 7-AAD Viability Staining Solution (420,403, BioLegend) for 10 min at room temperature and then incubated with cell-surface antibodies for 30 min on ice. The following monoclonal antibodies were used: anti-CD3-PE-Cy7 (300,420, BioLegend), anti-CD8-Alexa Fluor® 700 (561,453, BD Biosciences). Cells were identified using an LSRfortessa flow cytometer (BD Biosciences) and data were assessed using FlowJo software (FlowJo).

Immunofluorescence assay

A sample of 2.5×10^5 isolated PBMCs was grown in a 96-well plate in 200 mL of the complete medium combined with or without 50 ng/mL of LMO5 or 40 nM tofacitinib. Following incubation at 37 °C for 4 days without recycling the medium, the PBMCs were obtained and resuspended in 500 mL of PBS. An aliquot of 2 mL of cell suspension was pipetted onto a slide and allowed to dry. The cells were permeabilized and blocked in PBS containing 5% normal goat serum (SL038, Solarbio) and 0.3% Triton X-100 (V900502, Vetec) for 1 h at room temperature. The cells were incubated with a primary antibody against CD8 (1:100; ab237709, Abcam) and Phospho-Stat3 (1:50; 4113S, CST) overnight at 4 °C. Following 3 washes in PBS, the sections were incubated with Alexa Fluor® 488-conjugated anti-rabbit IgG (H + L) (1:500; 4412S, CST) and Alexa Fluor® 594-conjugated anti-mouse IgG (H + L) (1:500; 8890S, CST), for 1 h at room temperature. Additionally, DAPI (1:2000; Sigma, 32,670) was employed to stain cell nuclei. Slides were mounted using Fluoro-Gel (17985-10, Electron Microscopy Sciences, Hatfield, PA, USA) and imaged using an Olympus IX71 fluorescence microscope (Olympus).

Statistical analysis

The Shapiro-Wilk test was utilized to assess the normality of the data. If the data exhibited normal distribution, the means of two groups were compared using Student's test; otherwise, the Mann-Whitney U test was employed. For the comparison of three groups, one way analysis of variance (ANOVA) with post hoc Tukey's tests were conducted. A *p*-value or adjusted *p*-value below 0.05 was deemed to indicate statistical significance.

RESULTS

Clinical outcomes and responses to tofacitinib

Our scRNA-seq analysis suggested that the JAK-STAT pathway could be a potential therapeutic target for the index patient. With informed consent from his family, the patient was initiated on 5 mg/day of tofacitinib, a JAK1 and JAK3 inhibitor. After confirming the absence of toxicity, the dosage of tofacitinib was increased to 10 mg/day two weeks later. Two months into the tofacitinib treatment, the patient exhibited a favorable response (Fig. 1A): the CASE score decreased to 8 (Supplemental table 1), brain lesions reduced in MRI (Fig. 1B(c, d)), brain periodic spikes disappeared in EEG (Supplemental Fig. 1B), GABAAR-IgG titers decreased in serum and CSF (Supplemental Fig. 2C). Following family consent, the mediastinal tumor was surgically resected, histological examination confirmed the diagnosis of thymoma (B1 type) (Fig. 1D). Subsequently, the patient continued to received treatment with prednisolone and tofacitinib, and was followed up for 14 months, during which the clinical condition slowly improved (Supplemental video 1–8).

scRNA-seq analysis uncovers cell-mediated immunity activation in anti-$GABA_A$-R encephalitis

Following unsupervised clustering and t-distributed stochastic neighbor (t-SNE) plot analyses (Fig. 1E), cluster identities were determined by the expression of established markers (Fig. 1F, Supplemental table 2), indicating successful capture of major peripheral blood mononuclear cell (PBMC) subsets. Projection of the numbers of differentially expressed genes (DEGs) between patient- and four healthy volunteers (HVs)-derived cells revealed broad transcriptomic alterations observed in T cells and monocytes. Notably, the most prominent transcriptomic changes were observed in the effector $CD8^+$ T cell cluster (Fig. 1G).

To understand the biological significance of transcriptional changes in the effector $CD8^+$ T cell cluster, we conducted pathway enrichment analysis with DEGs. This analysis revealed enrichment of pathways related to T cell activation and interferon-gamma signaling, driven, in part, by the upregulation of *JAK2*, *JAK3*, and *STAT1* (Fig. 1H, I). Dysregulation of JAK-STAT signaling has been strongly associated with immune activation [3]. Subclustering of the effector $CD8^+$ T cell resulted in the segregation of the patient and HV clusters, demonstrating distinct transcriptomic differences

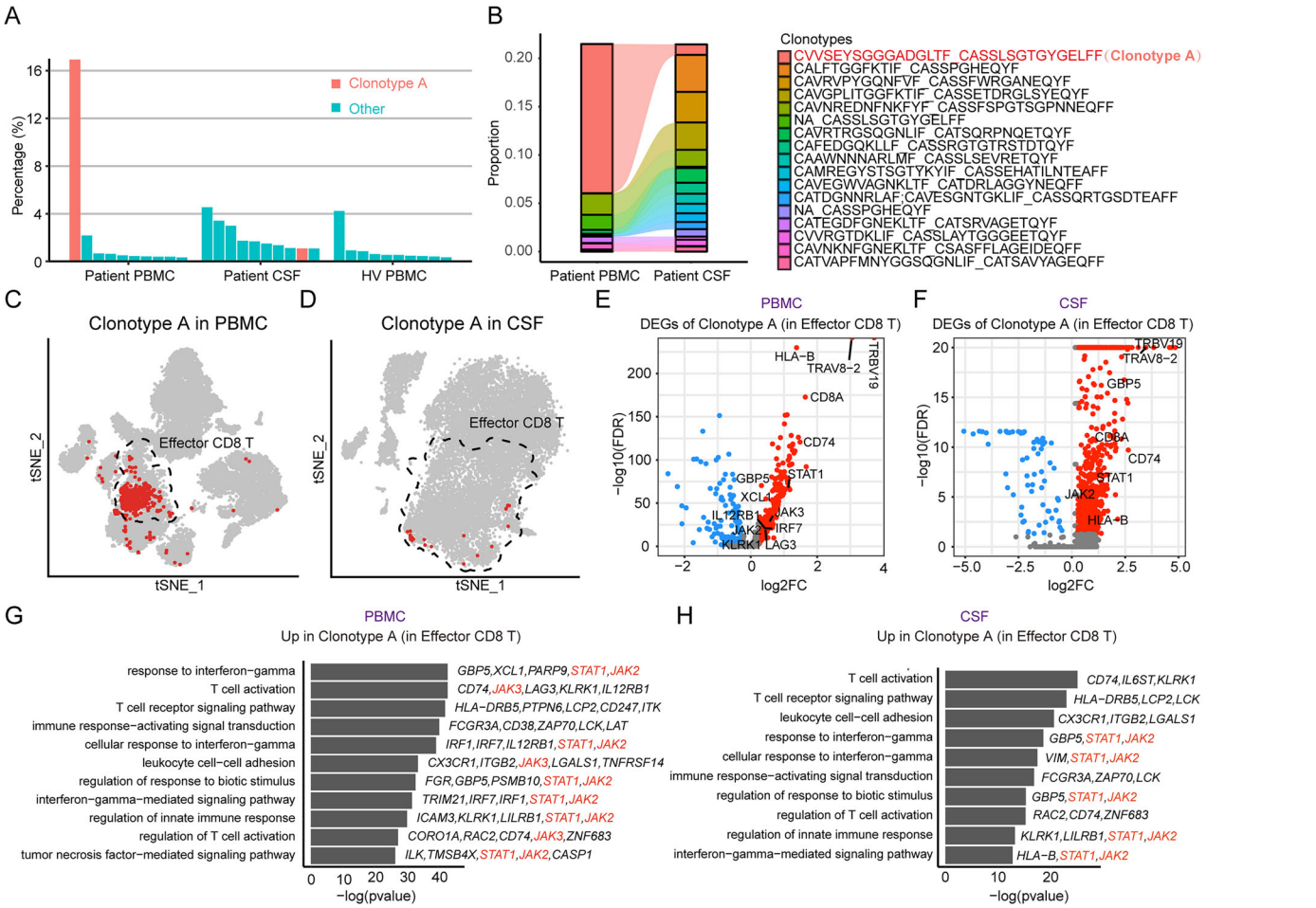

Fig. 2 Unique TCR utilization in effector CD8 T cells of an anti-GABA$_A$ receptor encephalitis patient. A Bar plot illustrating the distribution of the Top 1 clonotype (named clonotype A, red) of Patient PBMCs in Patient CSF, and HV PBMC. **B** Alluvial plot illustrating the top 20 clonotypes between patient PBMC and patient CSF. **C** The t-SNE plot projection of PBMCs from Patient and HV, with cells in clonotype A labeled in red and Effector CD8 T cells indicated with a dashed line. **D** The t-SNE plot projection of CSF cells from Patient and HV, with cells in clonotype A labeled in red, and Effector CD8 T cells indicated with a dashed line. **E** Volcano plot illustrating DEGs that are up- or down-regulated in Clonotype A of PBMC Effector CD8 T cells, with notable DEGs labeled. **F** Volcano plot illustrating DEGs that are up- or down-regulated in Clonotype A of CSF Effector CD8 T cells, with notable DEGs indicated. **G** GO enrichment analyses of DEGs in **E** Bar plot showing up-regulated GO terms in clonotype A cells and notable genes indicated in red. The *p*-value was derived using a hypergeometric test. **H** GO enrichment analyses of the DEGs in **F** Bar plot illustrating the up-regulated GO terms from clonotype A cells and notable genes labeled in red. The *p*-value was derived using a hypergeometric test.

(Fig. 1J). This further validated that the expression of the *JAK2*, *JAK3*, and *STAT1* was upregulated in the patient PBMC cluster. Additionally, *JAK2*, *JAK3*, and *STAT1* were also upregulated in the effector CD8$^+$ T cell cluster of CSF (Supplemental Fig. 3A–F, Supplemental table 3). Consequently, the JAK-STAT signaling pathway emerged as a potential therapeutic target.

Single-cell T cell receptor (TCR) sequencing demonstrates unique TCR usage in effector CD8$^+$ T cells of anti-GABA$_A$-R encephalitis

To investigate the clonality of T cells in PBMCs and CSF from the patient, we conducted single-cell TCRβ CDR3 sequencing using the Chromium Single Cell Immune Profiling platform. The results revealed that, in the patient, the top TCR clone "CDR3: CVVSEYSGGGADGLTF_CASSLSGTGYGELFF" (referred as clonotype A T cells) constituted more than 16% of PBMC T cells, approximately eight times that of the second-highest clone (Fig. 2A, Supplemental table 4). In contrast, in HV, the top clone comprised only 7% of PBMC T cells, less than twice that of the second-highest clone. This indicated the presence of a unique TCR clone in the patient's PBMC T cells. Additionally, clonotype A T cells were also found in the patient's CSF, suggesting that these cells might have crossed the blood-brain barrier to enter the CSF (Fig. 2B). When projected onto the t-SNE plots, clonotype A T cells in PBMC were predominantly identified as effector CD8$^+$ T cells (Fig. 2C). Similarly, clonotype A T cells in the CSF were also characterized as effector CD8$^+$ T cells (Fig. 2D). Comparative analysis revealed the upregulation of *JAK2*, *JAK3*, and *STAT1* in clonotype A T cells compared to other effector CD8$^+$ T cells in PBMC (Fig. 2E, G), and CSF (Fig. 2F, H). These findings underscored that clonotype A T cells were the primary cell type exhibiting the highest JAK-STAT signaling activation.

Tofacitinib suppresses CD8$^+$ T cell proliferation caused by LMO5 derived from the thymoma of an anti-GABA$_A$-R encephalitis patient

It has been reported that LIM-domain-only protein 5 (LMO5), acting as a tumor antigen associated with cell-cycle regulation and tumor growth, cross-reacts with autoantibodies to GABA$_A$-R(5). To investigate this relationship, we conducted dot blot analysis to examine the interaction between autoantibodies in the patient's serum and LMO5. As depicted in Fig. 3A, autoantibodies in the

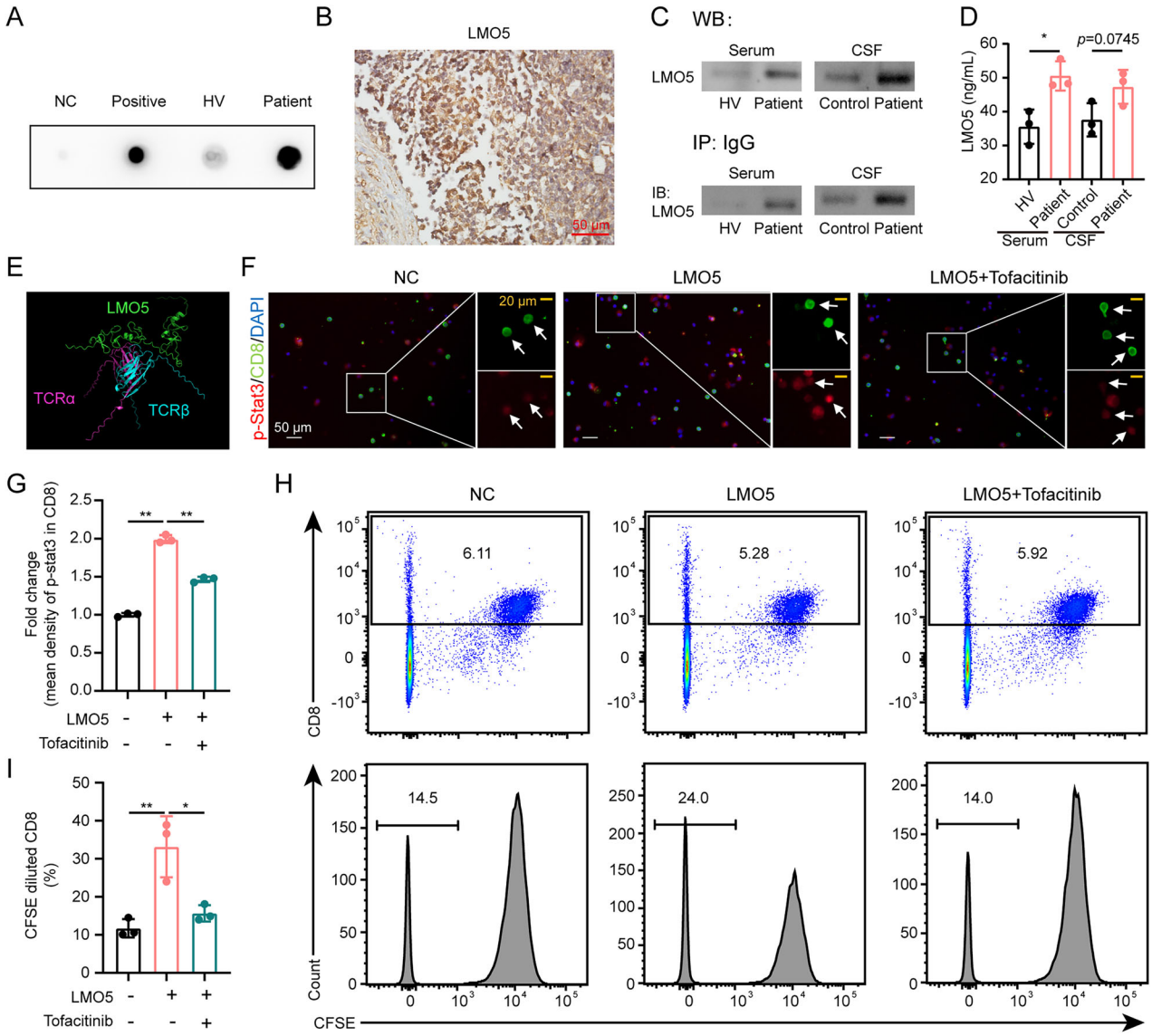

Fig. 3 Inhibition of LMO5-induced CD8 T cell proliferation through the use of tofacitinib. A Dot blot using the serum of the patient and HV to identify LMO5-IgG. Commercial LMO5 antibodies were used as the positive control; NC was the negative control. **B** Immunohistochemistry of LMO5 in the thymoma of anti-$GABA_A$ receptor encephalitis. **C** Western blot of LMO5 on serum from HVs and the patient and CSF from control and the patient ($n = 3$); immunoprecipitation results from a LMO5 immunoblot after human IgG immunoprecipitation ($n = 3$). **D** Concentration of LMO5 in serum and CSF via ELISA ($n = 3$). **E** The 3D molecular structures of docking result, computationally predicted by ZDOK, between LOM5 (green) and TRA (red), and TRB (blue) from clonotype A. **F** Immunofluorescence of phosphorylated Stat3 (p-Stat3, red) and CD8 (green) in PBMC treated with LMO5 (50 ng/mL) or LMO5 (50 ng/mL) plus tofacitinib (40 nM). Nuclei were counterstained using DAPI (blue) ($n = 3$). **G** Statistical examination of relative mean fluorescence intensity of p-Stat3 in CD8-positive cells in **F**. $^{**}p < 0.01$, one-way ANOVA using a post hoc Tukey's test. **H** Flow cytometry detection of CD8+ T cell proliferation through a lymphocyte transformation test (LTT). CFSE-labeled PBMCs were cultured alongside LMO5 (50 ng/mL) or LMO5 (50 ng/mL) plus tofacitinib (40 nM) for six days ($n = 3$). **I** Quantification of CD8+ cell proliferation in **H**. $^{*}p < 0.05$, $^{**}p < 0.01$, one-way ANOVA using a post hoc Tukey's test.

patient's serum specifically recognized LOM5. Subsequently, we confirmed the presence of LOM5 in the resected thymoma through immunohistochemistry (Fig. 3B). Moreover, we observed higher levels of LMO5 in the patient's serum and CSF respectively (Fig. 3C, D; Supplemental Fig. 5).

To delve into the role of LMO5 in anti-$GABA_A$-R encephalitis, we explored its potential binding to TCR in clonotype A T cells using ZDOK (Fig. 3E; binding score provided in Supplemental table 5). Given the activation of the JAK-STAT signaling pathway in clonotype A CD8+ T cells, we hypothesized that LMO5 might influence this pathway in $CD8^+$ T cells.

Figure 3F, G illustrate that LMO5 enhanced the expression of phospho-Stat3 (p-Stat3), a key indicator of the JAK-STAT signaling pathway, in $CD8^+$ T cells, suggesting that LMO5 could activate the JAK-STAT signaling pathway. Furthermore, Tofacitinib reversed the increased expression of p-Stat3. Activation of the JAK-STAT signaling pathway can lead to the proliferation of $CD8^+$ T cells, intensifying inflammatory reactions. In line with this, we observed that LMO5 induced the proliferation of $CD8^+$ T cells (Fig. 3H, I). Notably, Tofacitinib suppressed the proliferation of $CD8^+$ T cells induced by LMO5 in vitro.

DISCUSSION

In this study, scRNA-seq was conducted on PBMC and CSF of a 42-year-old male patient with refractory anti-$GABA_A$-R encephalitis

and thymoma. The analysis identified the JAK-STAT signaling pathway as a potential target. The patient received the JAK inhibitor tofacitinib, resulting in a notable improvement in clinical outcomes. This suggests that tofacitinib may have an intervention effect on the pathogenesis of anti-$GABA_A$ receptor encephalitis, highlighting the potential of scRNA-seq analyses in advancing personalized medicine for such patients.

While previous studies primarily focused on humoral immunity [4–6], a group provided evidence for a significant role that CD8+ T cells may play in the pathogenesis [7]. Recently, tissue-resident CD8+ T cells were found to be essential drivers of chronic CNS autoimmunity [8]. Our scRNA-seq analysis uncovered broad transcriptomic changes in various T cell types, with the most significant alterations observed in the effector CD8+ T cells cluster. Pathway enrichment analysis revealed upregulated genes associated with the JAK-STAT signaling pathway, T-cell activation, and inflammatory response signaling in these effector CD8+ T cells, consistent with prior reports linking the JAK-STAT signaling pathway to T-cell activation [9, 10]. Additionally, single-cell TCR sequencing identified a highly monoclonal TCR repertoire in $CD8^+$ T cells from the patient. Upregulation of *JAK2*, *JAK3*, and *STAT1* was also identified in the specific monoclonal effector $CD8^+$ T cells. Therefore, we have demonstrated that a group of specific monoclonal effector $CD8^+$ T cells and abnormal JAK-STAT signaling pathways are involved in the disease.

Further investigation into potential upstream molecules activating the JAK-STAT signaling pathway led us to explore LOM5, a tumor antigen. Previous reports indicated LOM5's cross-reactivity with autoantibodies to anti-$GABA_A$-R [4]. In our study, elevated expression of LOM5 was identified in peripheral blood, CSF, and thymoma from the patient. Bioinformatic analysis predicted LMO5's binding to monoclonal TCR, suggesting its role in driving the immune process. LOM5-induced T cell proliferation, as demonstrated by the lymphocyte transformation test, supported the hypothesis that $CD8^+$ T cell-mediated early antitumor responses may release intracellular proteins including LOM5, triggering the production of $GABA_A$-R autoantibodies.

Furthermore, we observed higher p-Stat3 expression in $CD8^+$ T cells cultured with LOM5, which was reduced in $CD8^+$ T cells treated with tofacitinib. This led to the hypothesis that LMO5 induces $CD8^+$ T cell activation through the JAK-STAT signaling pathway, and tofacitinib suppresses LMO5-induced $CD8^+$ T cell proliferation in vitro. Collectively, our results suggest that the JAK-STAT signaling pathway may serve as a potential therapeutic target for Anti-$GABA_A$ receptor encephalitis.

Notably, targeting the JAK-STAT signaling pathway with JAK inhibitors, such as tofacitinib, has shown success in various autoimmune and inflammatory diseases [11, 12]. The favorable response to tofacitinib in our refractory case aligns with the emerging use of JAK inhibitors in treating rare cases of autoimmune or inflammatory diseases [11, 13, 14]. The successful intervention with tofacitinib in our case also demonstrated aberrant JAK-STAT activity in anti-$GABA_A$-R encephalitis.

In conclusion, our results for the first time revealed specific monoclonal effector $CD8^+$ T cells and abnormal JAK-STAT signaling pathway activation in refractory anti-GABAA-R encephalitis. The successful intervention with tofacitinib supports the consideration of the JAK-STAT pathway as a potential therapeutic target in this disease. Nonetheless, these findings warrant further investigation in a larger patient cohort to validate their broader applicability.

DATA AVAILABILITY

The raw sequence data of PBMC single-cell RNAseq data reported in this paper have been deposited in the Genome Sequence Archive (*T. Chen,* et al., *The Genome Sequence Archive Family: Toward Explosive Data Growth and Diverse Data Types. Genomics, Proteomics & Bioinformatics 2021;* ***19****, 578–583*) in National Genomics Data Center (*C.-N. Members, Database Resources of the National Genomics Data Center, China National Center for Bioinformation in 2023. Nucleic acids research 2023; 51, D18–D28.*), China National Center for Bioinformation/ Beijing Institute of Genomics, Chinese Academy of Sciences (GSA-Human: HRA006109) that are publicly accessible at https://ngdc.cncb.ac.cn/gsa-human. The raw sequence data of CSF single-cell RNAseq data (GSE138266) from the public 5 idiopathic intracranial hypertension subjects cited in this paper have been deposited in https://www.ncbi.nlm.nih.gov/pmc/articles/PMC6959356/.

REFERENCES

1. Spatola M, Petit-Pedrol M, Simabukuro MM, Armangue T, Castro FJ, Barcelo AM, et al. Investigations in GABA(A) receptor antibody-associated encephalitis. Neurology. 2017;88:1012–20.
2. Petit-Pedrol M, Armangue T, Peng X, Bataller L, Cellucci T, Davis R, et al. Encephalitis with refractory seizures, status epilepticus, and antibodies to the GABAA receptor: a case series, characterisation of the antigen, and analysis of the effects of antibodies. Lancet Neurol. 2014;13:276–86.
3. Xue C, Yao Q, Gu X, Shi Q, Yuan X, Chu Q, et al. Evolving cognition of the JAK-STAT signaling pathway: autoimmune disorders and cancer. Signal Transduct Target Ther. 2023;8:204.
4. Brandle SM, Cerina M, Weber S, Held K, Menke AF, Alcala C, et al. Cross-reactivity of a pathogenic autoantibody to a tumor antigen in GABA(A) receptor encephalitis. Proc Natl Acad Sci USA. 2021;118:e1916337118.
5. Ohkawa T, Satake S, Yokoi N, Miyazaki Y, Ohshita T, Sobue G, et al. Identification and characterization of GABA(A) receptor autoantibodies in autoimmune encephalitis. J Neurosci. 2014;34:8151–63.
6. Kreye J, Wright SK, van Casteren A, Stoffler L, Machule ML, Reincke SM, et al. Encephalitis patient-derived monoclonal GABAA receptor antibodies cause epileptic seizures. J Exp Med. 2021;218:e20210012.
7. Bracher A, Alcala C, Ferrer J, Melzer N, Hohlfeld R, Casanova B, et al. An expanded parenchymal CD8+ T cell clone in GABA(A) receptor encephalitis. Ann Clin Transl Neurol. 2020;7:239–44.
8. Frieser D, Pignata A, Khajavi L, Shlesinger D, Gonzalez-Fierro C, Nguyen XH, et al. Tissue-resident CD8(+) T cells drive compartmentalized and chronic autoimmune damage against CNS neurons. Sci Transl Med. 2022;14:l6157.
9. Fortelny N, Farlik M, Fife V, Gorki AD, Lassnig C, Maurer B, et al. JAK-STAT signaling maintains homeostasis in T cells and macrophages. Nat Immunol. 2024;25:847–59.
10. Meyer LK, Verbist KC, Albeituni S, Scull BP, Bassett RC, Stroh AN, et al. JAK/STAT pathway inhibition sensitizes CD8 T cells to dexamethasone-induced apoptosis in hyperinflammation. Blood. 2020;136:657–68.
11. Jamilloux Y, El JT, Vuitton L, Gerfaud-Valentin M, Kerever S, Seve P. JAK inhibitors for the treatment of autoimmune and inflammatory diseases. Autoimmun Rev. 2019;18:102390.
12. Damsky W, Peterson D, Ramseier J, Al-Bawardy B, Chun H, Proctor D, et al. The emerging role of Janus kinase inhibitors in the treatment of autoimmune and inflammatory diseases. J Allergy Clin Immunol. 2021;147:814–26.
13. Jang Y, Lee WJ, Lee HS, Chu K, Lee SK, Lee ST. Tofacitinib treatment for refractory autoimmune encephalitis. Epilepsia. 2021;62:e53–e59.
14. Dinoto A, Ferrari S, Mariotto S. Treatment Options in Refractory Autoimmune Encephalitis. Cns Drugs. 2022;36:919–31.

ACKNOWLEDGEMENTS

The authors wish to thank Xianhui Dong (IEMed Guangzhou Biomedical Technology Co. Ltd) for his technical assistance. The authors also would like to thank the patient and the volunteer healthy controls for their participation. The current study was supported by the National Natural Science Foundation of China (82371354, 82071343, 81701188, 81971140, 82271377), and the Guangzhou Science and Technology Key R&D Plan (2023B03J1347), and Guangzhou Municipal School (Hospital) Joint Funding (202201020415), the Guangdong Basic and Applied Basic Research Fund (2021A1515010393).

AUTHOR CONTRIBUTIONS

Conception and design of the study: YQS, ZXH, HFP and WQ; Acquisition and analysis of data: YQS, HFP, YH, QHL, HLL, ZBL, JLY, LF, JNC, JFL, YL, ZHW, JL, YJL, ZQL, LBL; Drafting a significant portion of the manuscript or figures: YQS, ZXH, YH and HFP.

COMPETING INTERESTS

The authors declare no competing interests.

ADDITIONAL INFORMATION

Supplementary information The online version contains supplementary material available at https://doi.org/10.1038/s41398-025-03300-y.

Correspondence and requests for materials should be addressed to Yaqing Shu, Zhongxi Huang, Fuhua Peng or Wei Qiu.